Unperturbed Archean lithosphere beneath the Eastern Dharwar Craton Kimberlite Field, India: inferred from joint inversion of surface wave dispersion and receiver function data

D. K. Chaubey[1], S. S. Rai[1], N. Mullick[1] and R. Das[2]

[1] Department of Earth and Climate Science, Indian Institute of Science Education & Research Pune, India, [2] Department of Earth Sciences, Pondicherry University, Pondicherry, India

Corresponding author: Dipak Chaubey (dipakchaubey26@gmail.com)

Highlights:

- Evidence for a 175 km thick lithosphere beneath the Archean Eastern Dharwar craton.
- The lithosphere has a shear wave velocity of 4.7-4.8 km/s, typical for a craton.
- Moderate coupling between the Dharwar craton lithosphere and asthenosphere.
- Collocated seismological and kimberlite xenolith data reveal undisturbed craton root.

Abstract

Cratons are the oldest part of the continent, began to form about 3 Ga ago, and remained stable for over a billion years. Many of them, however, are also susceptible to deformation and erosion under the influence of various geological processes. Diamondiferous kimberlites are a proxy for the existence of thicker and colder lithosphere at the time of their eruption, while the seismologically derived velocity model represents the present-day state of the lithosphere. The two observations together help understand the temporal evolution of the continent. We investigate the lithosphere-asthenosphere system beneath a 200 km long corridor at the 3.2-2.5 billion years old Eastern Dharwar Craton, South India, and its 1100 million years old diamondiferous kimberlite province with high-resolution shear wave velocity computed at ~15 km spacing through joint inversion of receiver function and surface wave phase dispersion data. The velocity model suggests a ~170-180 km thick lithosphere, characterized by high shear velocity (4.7-4.8 km/s) representative of an Archean craton, correlating with the kimberlite xenolith data. Our result suggests no major thermal alteration to the Archean lithosphere of the Eastern Dharwar craton despite being affected by kimberlite volcanism, Marion mantle plume, and fast motion of the Indian plate for 140 million years. The lithosphere-asthenosphere boundary is 50 km wide with a velocity drop of ~2%, suggesting moderately low viscosity (velocity) asthenosphere below the high viscosity (velocity) craton consistent with the continental undertow model. These studies suggest that the Eastern Dharwar Craton has been moving with a thick root for 140 million years as part of the Indian continent and remains undeformed.

Keywords: Craton, lithosphere, Kimberlite, Seismology, Shear wave velocity, Dharwar craton

1. Introduction

Cratons - the oldest part of continents formed during the Precambrian, are 150-255 km thick, cold, buoyant regions of the Earth that has remained stable for more than a billion year (Boyd et al., 1985; Pearson et al., 2021). They are composed of a depleted (high Mg#) mantle, geophysically characterized by a high shear wave velocity (Vs) and low heat flow (Hawkesworth et al., 1990; Jordan, 1988; Lee et al., 2011; Sleep, 2005). Melt depleted composition of the cratonic lithosphere leads to positive chemical buoyancy that offsets the negative thermal density of cold mantle material. The high viscosity lithosphere is underlain by the low viscosity asthenosphere. The nature of the mechanical coupling between the cratonic root with the underlying asthenospheric mantle is a subject of several investigations (Alvarez, 1982, 1990; Lenardic et al., 2003; Paul et al., 2019). The high viscosity of lithospheric keel and its coupling with the underlying mantle reduces the basal drag force acting on the cratonic root which stabilizes them against erosion by convective stresses and localized deformations leading to its longevity (Eeken et al., 2018; Lenardic et al., 2000; Yoshida & Yoshizawa, 2021). This continental undertow model was first conceptualized by Alvarez (1982, 1990) and explains the motion of a continental plate with a thick root driven by the underlying mantle convection. Though the Proterozoic mobile belt shields the cratonic core from later tectonomagmatic activity, they are nevertheless subject to reworking and destruction by various geological processes (Foley, 2008; Lee et al., 2011; Liu & Li, 2018; Wu et al., 2014).

An accurate description of the structure of the craton's lithosphere-asthenosphere (LA) system is critical to geodynamic modeling of the global mantle flow and elucidating the origin and evolution of continents and their role in the fast movement of the plate (Gerya, 2014; Yoshida & Yoshizawa, 2021). We present a robust estimate of the LA system from the eastern segment of the Dharwar craton, South India, (Figure 1) which has been subject to kimberlite volcanism at 1100 Ma, part of the fast-moving Indian plate for the last 140 Ma, and interacted with the Marion mantle plume at 90 Ma. There are contrasting views on the effect of these prolonged tectonic activities on the physical-thermal status of the Indian lithosphere, such as erosion of the Indian lithosphere responsible for the fast movement of the Indian plate (Kumar et al., 2007, 2013; Liu & Li, 2018; Maurya et al., 2016) *vs* the preserved pristine Archean lithosphere supporting the drifting continent with deep cratonic root (Mitra et al., 2006; Priestley et al., 2021; Saha et al., 2020).

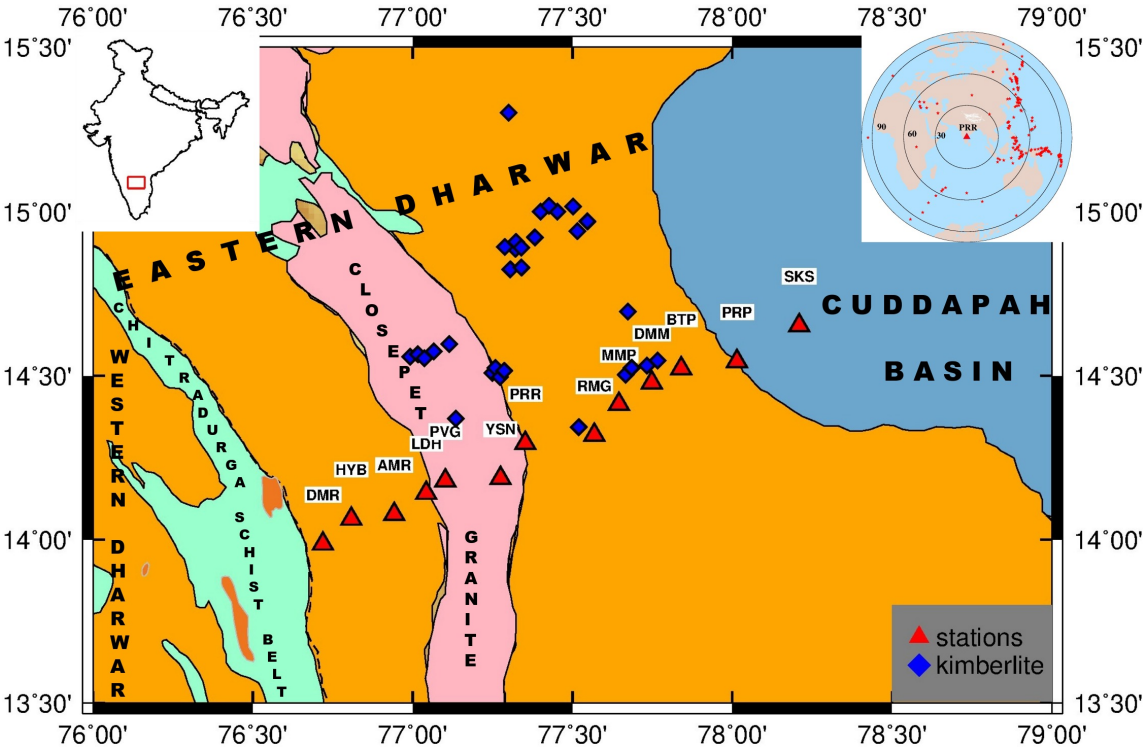

Figure 1. Simplified geological map of the Eastern Dharwar craton and Cuddapah basin along with the locations of kimberlite pipes and seismological stations used in this study. Insets show the location of the study region within India (top left) and the distribution of the earthquakes (M >5.5) used in receiver function computation (top right). Details of the seismological stations are provided in Supplementary Table 1 and Saikia et al. (2017).

We combined collocated seismological and kimberlite xenolith data to explore the internal structure of the region encompassing an undisturbed Archean segment, a diamondiferous kimberlite domain, and a Paleo-Meso Proterozoic basin (Figure 1). Seismological observations provide information on the cratonic lithosphere's present-day physical, chemical, and thermal status. The kimberlite xenoliths are a more direct source of information about the composition and thermal state of the lithospheric mantle at its time of eruption (Foley et al., 2019; Pearson et al., 2019). We investigate here the upper mantle velocity architecture of the mid-to the late- Archean Eastern Dharwar craton (EDC) (Goodwin, 1996; Naqvi & Rogers, 1987) beneath a 200 km long profile with dense (~15 km station spacing) network of broadband seismographs operated during 2012-14 (Figure 1).

2. Geological framework

The Dharwar craton, in the southern part of India, is dominantly an Archean

terrain composed of tonalite-trondhjemite-granodiorite (TTG) gneisses, greenstone belts, and calc-alkaline to potassic granitoid (reviewed in Goodwin, 1996; Naqvi & Rogers, 1987). Based on U–Pb zircon ages and Nd isotope data, and crustal lithology, the craton is divided into Western Dharwar Craton (WDC) underlain by old crust (3400–3000 Ma) composed of older TTG gneisses and volcanic-sedimentary greenstone sequences, and the Eastern Dharwar Craton (EDC) with mainly younger (2700–2520 Ma) crust composed of different type of granitoid overlayed with narrow ~2.7 Ga greenstone belts (Chadwick et al., 2000; Chardon et al., 2011; Peucat et al., 2013; Jayananda et al., 2020). The Western and Eastern Dharwar cratons are separated by the eastern margin of the Chitradurga greenstone belt (Swaminath and Ramakrishnan, 1981).

The study area is situated in the EDC, extending from the Chitradurga schist belt in the West to the Proterozoic Cuddapah Basin in the East (Figure 1). Its central part covers the 1023 Ma to 1125 Ma age kimberlite fields (Kumar et al., 2007) emplaced within the Archean (3300-2550 Ma) granite and granite gneiss. Systematic petrographic, geochemical, and thermo-barometric studies on the kimberlite drill core samples reveal xenolith composition from pyroxene to dunite (Ganguly & Bhattacharya, 1987). It also includes garnet-harzburgites, lherzolites, wehrlites and olivine clinopyroxenites along with spinel and a wide presence of phlogopites. The Mg/(Mg+Fe) ratio of olivines in the EDC kimberlite xenoliths has a very restricted range of 0.91-0.94 and slightly lower up to 0.82 in the kimberlite matrix, implying a difference in the mantle composition. Based on the positive relation between Cr/(Cr+Al) and Mg/(Mg+Fe) in the kimberlite xenoliths, Ganguly and Bhattacharya (1987) suggest a progressively increase in mantle fertility with increasing depth. Their major conclusions from the mantle thermal gradient based on the P-T condition of equilibration of coexisting minerals in the xenoliths are (i) the ultrabasic and eclogite extraction from depths of 70-150 km and 100-185 km, (ii) the lithosphere thickness of 185 km during mid-Proterozoic at the time of kimberlite eruption, similar to those of the African cratons. These inferences are validated by subsequent studies by Griffin et al. (2009) and Shaikh et al. (2020).

3. Previous Geophysical studies

The upper mantle structure of the EDC has not been investigated in detail using geophysical methods. Much of the information is based on regional surface wave studies (Bodin et al., 2014; Borah et al., 2014; Maurya et al., 2016; Mitra et al., 2006; Saha et al., 2020). The lithosphere thickness computed by these studies varies from 140 km to 185 km beneath EDC. On the contrary, Negi et al. (1986) used surface heat flow, and Kumar et al. (2007, 2013) based on the negative gradient of S receiver function amplitude at a few locations in South India, suggested a ~100 km thin lithosphere. These results were criticized by Oreshin *et al.* (2011), Kosarev et al., (2013), Bodin et al., (2014), and Krueguer et al., (2021) as arising from an inappropriate analysis and modeling of the data. Based on the joint inversion of multiple seismological data sets, the negative velocity gradient is attributed to a mid-lithospheric discontinuity (MLD). Saha

et al. (2020) modeled at least 160 km thick lithosphere beneath the EDC with a Vs >4.7 km layer in the depth of 80-130 km. The velocity images of McKenzie et al. (2015), Maurya et al. (2016), and others are laterally averaged in the Dharwar craton due to their low resolution (2^0x 2^0 or more). The surface heat flux distribution over Eastern Dharwar varies from 35 mWm^{-2} in the western part to 40 mWm^{-2} in the eastern part comprising the kimberlite zone (Roy & Rao, 2000).

4. Velocity modeling approach

Shear wave velocity is one of the most reliable geophysical parameters to characterize the lithosphere due to its primary dependence on the thermal state of the upper mantle (Jordan, 1979; Priestley & McKenzie, 2006; Schutt & Lesher, 2006). We computed the velocity structure to a depth of 300 km at 13 locations along the 200 km long profile at EDC through joint inversion of surface wave dispersion (SWD) with receiver function (RF) at 13 stations through the generalized damped least-squares inversion approach *joint96* (Herrmann, 2013). Detailed analysis of RF data, the Rayleigh wave dispersion measurement, and the inversion methodology are discussed below.

4.1 Receiver function computation

As teleseismic P-wave energy travels through the upper mantle and crust towards a seismic station, intervening seismic discontinuities cause a fraction of the P-wave energy converted to S-waves. These P-to- S converted phases and their reverberations, can be extracted from the source and propagation effects, by deconvolving the vertical component of the seismogram from the radial and transverse components. The resulting time series closely corresponds to the impulse response of the Earth structure beneath a seismic receiver and is called the P-wave receiver function (Langston 1977). The receiver function (RF) depends on Earth layer thickness, impedance contrast, and density, and is used to determine the Earth's properties. Several methods are used for extracting the Ps converted phases from the two horizontal components of the seismograms (Ammon 1991; Gurrola et al. 1995; Ligorria & Ammon 1999; Park & Levin 2000). The iterative time-domain deconvolution technique has been used in this paper (Ligorria and Ammon, 1999; Herrmann, 2013). This method assumes that the radial seismogram is a convolution of the vertical component with the Earth structure so that the latter can be isolated by extracting a time series which, when convolved with the vertical component, would approximate the horizontal component. This is accomplished by a least-square minimization of the difference between the observed horizontal seismogram and a predicted signal generated by the convolution of an iteratively updated spike train with the vertical.

The RF is computed from the waveforms of the earthquake (M_W 5.5) in the epicentral distance of 30°-100° for a Gaussian filter width of 1.6 corresponding to a maximum frequency of 0.9 Hz. The global distribution of earthquakes used in this study is shown in Figure 1(top right). Figure 2 (a, b) shows the behavior

of RF with varying epicenter distance and azimuthal at a station PRR. For selected stations, the RF behavior is presented in Supplement Figure S-1. The RF at individual stations is binned into different narrow distance-azimuth ranges and stacked to minimize noise and equalize the inhomogeneous distribution of observations. We restrict the distance and azimuth range to $\pm 10^0$ to reduce error due to Ps delay time variation and inhomogeneity below the station. Figure 2c to 2e show an example of stacking of RF for station PRR.

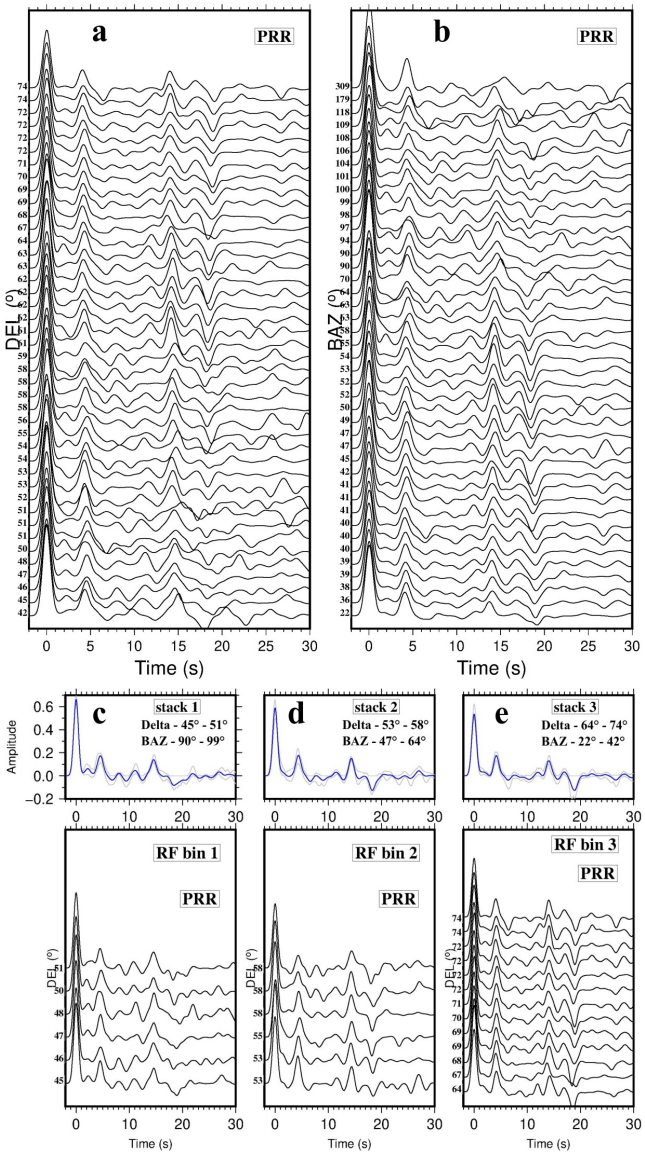

Figure 2. (a,b) Epicentral distance and azimuthal behavior of receiver func-

tions at station PRR computed at Gaussian width of 1.6, and (c-e) The bottom panel shows individual RF in a narrow distance-azimuth bin with the corresponding stacked RF in the top panel.

4.2 Surface wave dispersion data

Surface wave tomography using earthquake waveform has been widely used in the reconstruction of regional velocity images. Here, we compute the phase velocity dispersion directly from the earthquake waveforms following Jin and Gaherty (2015). In this approach, the relative phase delay of fundamental mode Rayleigh waves at different periods for different station pairs is calculated using waveform cross-correlation followed by computation of frequency-dependent phase delays (details in Gee & Jordan, 1992). We used longer period (40-140 s) dispersion data from Mullick et al. (2022) calculated following the approach of Jin and Gaherty (2015) from 846 regional and distant earthquakes (M >5.5) (Figure 3a) recorded over 85 broadband stations (Figure 3b).

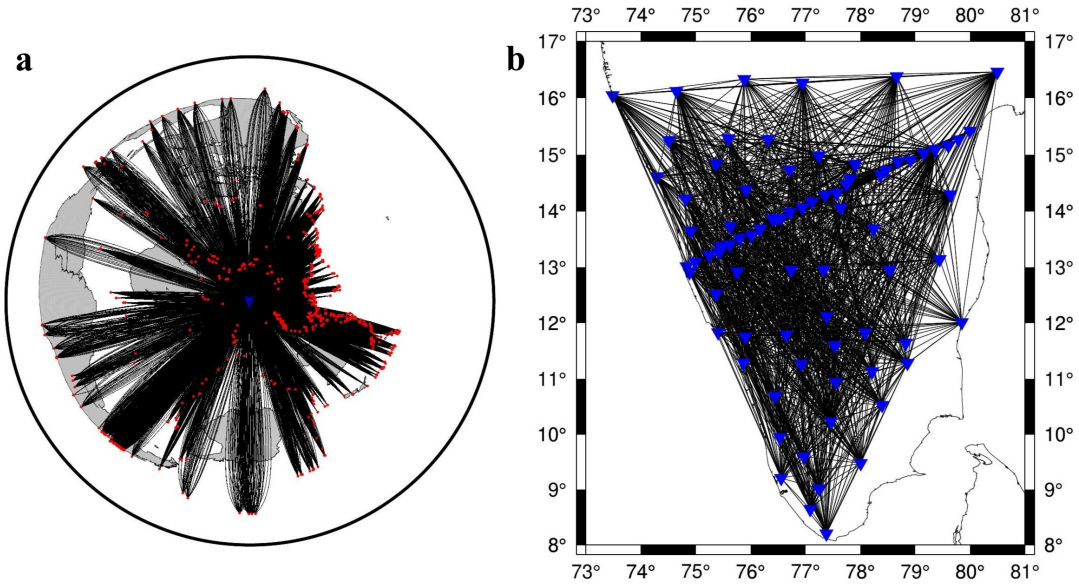

Figure 3. (a) Distribution of earthquakes (red) connecting stations on the great circle paths, and (b) Station distribution and inter-station links used to obtain phase velocity maps at periods 30-140s (Mullick et al., 2022). These stations were also used to compute a short period (2-30s) of the Rayleigh wave phase velocity map using ambient noise tomography (Das and Rai, 2017).

To accurately map the velocity structure of the lithosphere, a continuous phase velocity from shorter to longer periods is needed. In absence of high frequency in surface wave dispersion data, the inversion model to a depth of 80 km is influenced considerably by the local variation in the crustal velocity (Meier et al., 2007; Salaün et al., 2012). To avoid this, we included high frequency (2-30s) dispersion measurement through ambient noise tomography (Ritzwoller, 2009) applied to a network of stations (shown in Figure 3b). Details of methodology, model resolution, and velocity maps are presented in Das and Rai (2017). We combined the above-discussed results from Mullick et al (2022) and Das and Rai (2017) to generate a Rayleigh wave phase map in the period 2-140 s at a 0.5^0 grid interval, as shown in Figure 4 for selected periods.

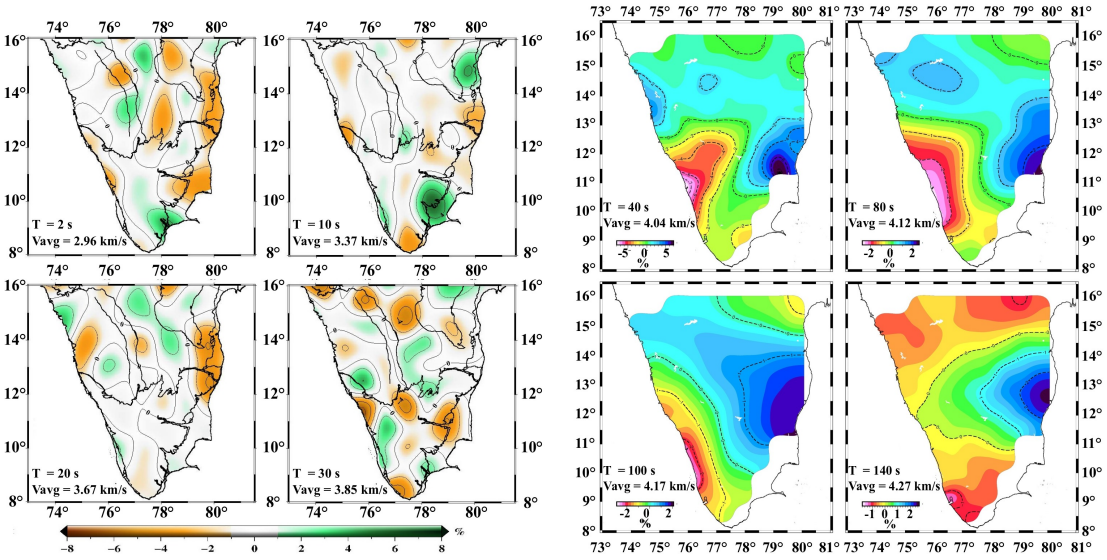

Figure 4. Rayleigh wave phase velocity map of the region at different periods presented as % deviation from the respective mean. The velocity maps at a shorter period of 2-30 s are taken from the ambient noise tomography results of

Das and Rai (2017). The longer period (40-140 s) phase velocity is from Mullick et al (2022).

4.3 Joint inversion approach

We computed the velocity-depth model at individual stations through the joint inversion procedure that combines the complementary constraints on S wave velocity by each data set into integrated velocity-depth profiles that match both sets of observations (Julia‘ et al., 2000). The dispersion velocities constrain absolute S wave velocity along frequency-dependent depth ranges, while receiver functions constrain relative velocity contrasts and vertical S-P travel times. The joint inversion procedure resulting models have a background velocity constrained by the dispersion values with the detailed variations constrained by the receiver functions superimposed. An additional benefit of the joint inversion scheme is that the nonuniqueness implicit in receiver function modeling (Ammon et al., 1990) is highly reduced with the addition of the surface wave dispersion information, and the final models have little dependence on the starting model (Julia‘ et al., 2000). The resultant velocity model is expected to minimize the joint prediction error given by,

$$|\Delta \mathrm{d}|^2 = \frac{(1-p)}{R} \sum_{i=1}^{R} \left(\frac{\Delta \mathrm{r}_i}{\sigma_{r_i}}\right)^2 + \frac{p}{S} \sum_{i=1}^{S} \left(\frac{\Delta \mathrm{s}_i}{\sigma_{s_i}}\right)^2$$

Where r_i refers to i^{th} of R number of RF samples, s_j is the S number of phase velocity. The parameter p determines the relative weighting between phase velocity and RF to the solution (Julia‘ et al., 2000). It varies from 0 for only RF to 1 for only SWD. The uncertainties ( ) are squared and thus contribute to the weighting of each datum more than p. As with any linearized inversion scheme, to stabilize the solution we add a damping parameter to the misfit function resulting in a trade-off between the final data fit and smoothness of the model $\Theta(\mathrm{m}) = \Delta \mathrm{d}^2 + \Theta^2 \cdot \mathrm{T}\Delta(\mathrm{m})^2$, where Θ^2 is a positive parameter called damping factor, Δm is a difference between the model in the current and previous iteration, and T is a Toeplitz matrix.

The inversion is performed using a number of parameters such as damping parameter, velocity models including Vp/Vs, and relative contribution of RF and SWD. We discuss here the basis for the choice of these parameters. The optimization process favors models with a small norm, which results in the damping of the model, that is, a smooth model. The optimum value of the damping parameter here is 0.5 computed using the L curve (Figure 5a). Inversion with a set of damping values from 0.1 to 1.0 shows model smoothing with increasing damping parameters (Figure 5b). Next, we evaluated the optimal value of parameter p examining the smoothness of the solution obtained for a number of p values from 0 to 1. The optimum value is p=0.3 (Figure 5c). Since the layer interface depth and Vp/Vs are held fixed during the inversion of dispersion data, we explored the effect of Vp/Vs in our inversion results (Figure 5d). Ear-

lier investigations based on analysis of RF and local earthquake studies suggest Vp/Vs vary from 1.73 to 1.80 (Rai et al., 2013; Saikia et al., 2017; Saikia and Rai, 2018). In this range, the joint inversion result changes only marginally and we chose Vp/Vs=1.73 for further analysis. We also explored the effect of initial velocity models e.g. half-space (with Vs of 4.5 km/s), AK135, IASP91, PREM, and Shapiro and Ritzwoller (2002) on the inversion result. The choice of the initial velocity model had no significant effect (Figure 5e). The inversion is performed considering a flat Earth model with a constant velocity of 4.5 km/s, comprising a stack of 2 km thick layers in the depth of 4-80 km and 5 km thick layers in the greater depth (80-300 km). The top 4 km is divided into 1 km thick layers to better resolve the low velocity in the shallowest depths.

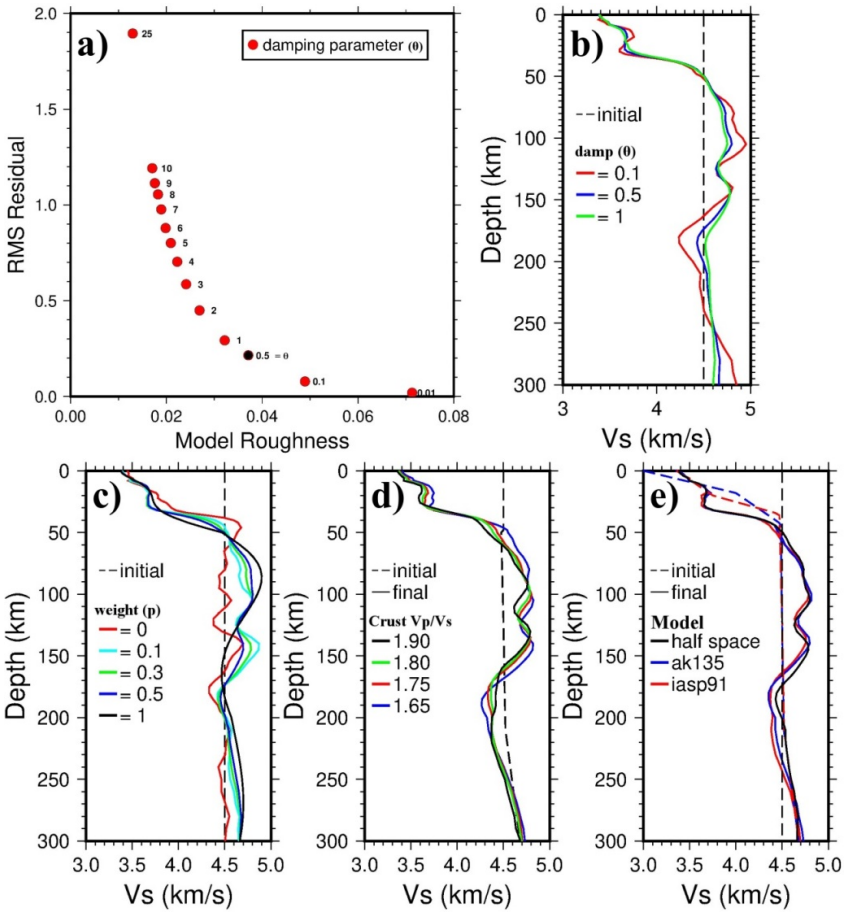

Figure 5. Computation of optimal parameters for joint inversion of RF and SWD. (a) L curve for optimal selection of damping parameter, (b) Influence of damping parameter on the inversion model, (c) Effect of relative weighting parameter between RF and SWD; p=0 is only RF and p=1 is only SWD, (d) Effect of Vp/Vs on inversion result, and (e) Inversion performed using different

initial velocity models.

The inversion of stacked RF time series at a station (binned in distance and azimuth range of $\pm 10^0$) and the corresponding dispersion data are performed in detail for a station PRR (Figure 6). To incorporate the effect of error in dispersion measurement we generate 100 random dispersion curves within ±5% of observed phase velocity dispersion at each station (Figure 6b inset). Each of these dispersion curves is then jointly inverted with each of 3 stacked RF (Figure 6a) to produce 300 velocity models. We narrowed the distribution of obtained 1-D velocity models by considering the 100 minimum error misfit solutions (Grey shades, Figure 6b) and chose their mean as a representative velocity model (Red line, Figure 6b). The inversion detail for other stations is presented in Supplementary Figure S-2. The velocity models for PRR show two negative velocity gradients (NVG): the first one from 4.7 to 4.6 km/s (1 to 2%) at a depth of 120-140 km (Figure 6b) and the other at a depth of 170-180 km.

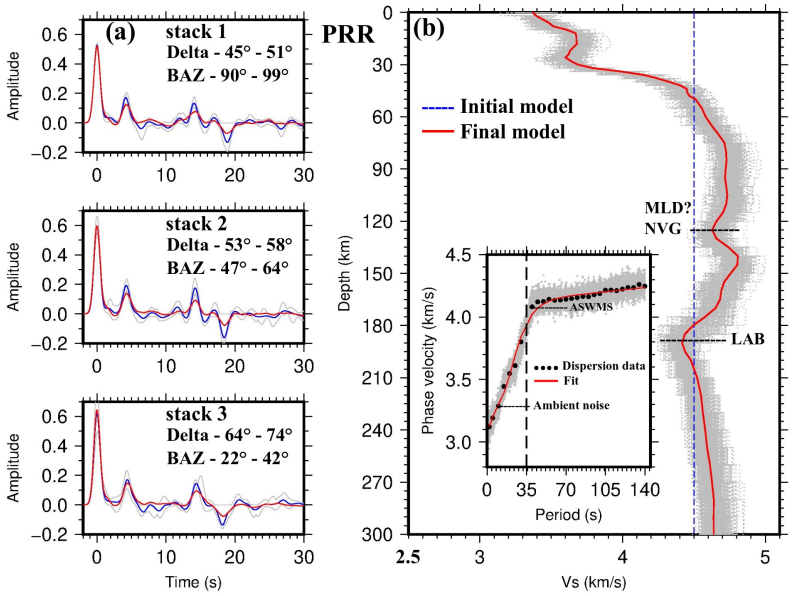

Figure 6. Joint inversion result at station PRR; a) Upper and lower bound of stacked RFs (in grey) along with their mean (blue) and the synthetic RF for the inverted model (red). b) Best 100 solutions (grey) from a set of 300 models computed considering 100 random Rayleigh wave dispersion curves (within 5% error bound shown in inset). The average of the 100 best solutions is shown as the red line.

5. Results

We compare velocity models from stations in the Dharwar kimberlite domain with other cratons like the Kaapvaal, Slave, Yilgarn (Pederson et al., 2009), and IASP91 (Figure 7a). The shear velocity in the EDC kimberlite domain (Figure

8a) increases progressively from 4.5 km/s at 50 km depth to a maximum of 4.75 km/s from 80 km to160 km, beyond which it decreases to a minimum of 4.5 km/s at 190 km. Subsequently, it increases progressively to 4.7 km/s at 300 km. At 130 km, we observe a marginally lower velocity (4.6 km/s). In the uppermost mantle (70-120 km), shear velocity in the kimberlite zone (> 4.7 km/s) is higher than that for many cratons (Figure 3a) while at more than 160 km depth the shear velocity is lower. These velocity characteristics are discussed below using varying composition (Figure 7b) and thermal gradients in the Earth (Figure 7c).

The velocity-depth model computed for lherzolitic to dunitic mantle composition (Bruneton et al., 2004; Eeken et al., 2018) predicts a maximum Vs of 4.8 km/s beneath the Moho at 50 km that progressively decreases (4.65-4.75 km/s) with depth due to gradual increase of temperature (Figure 7b). For a moderately metasomatized peridotite that contains phlogopite or amphibole, the Vs at 50 km depth is 4.5-4.65 km/s progressively decreasing to 4.3-4.4 km/s. The velocity models at EDC (kimberlite) match well with the theoretically predicted velocity for garnet harzburgite/webstrite composition of the upper mantle in the depth of 70-170 km, while its minimum velocity at a depth of 180-220 km could correspond to hydrated peridotite composition. In Figure 7c, we compare the observed shear velocity in the kimberlite domain with thermal gradients corresponding to surface heat flux of 30, 40, and 50 mW/m^2. In the 60-180 km depth, all the models compare to theoretically computed velocities for surface flux 30-40 mW/m^2 as observed over the kimberlite field.

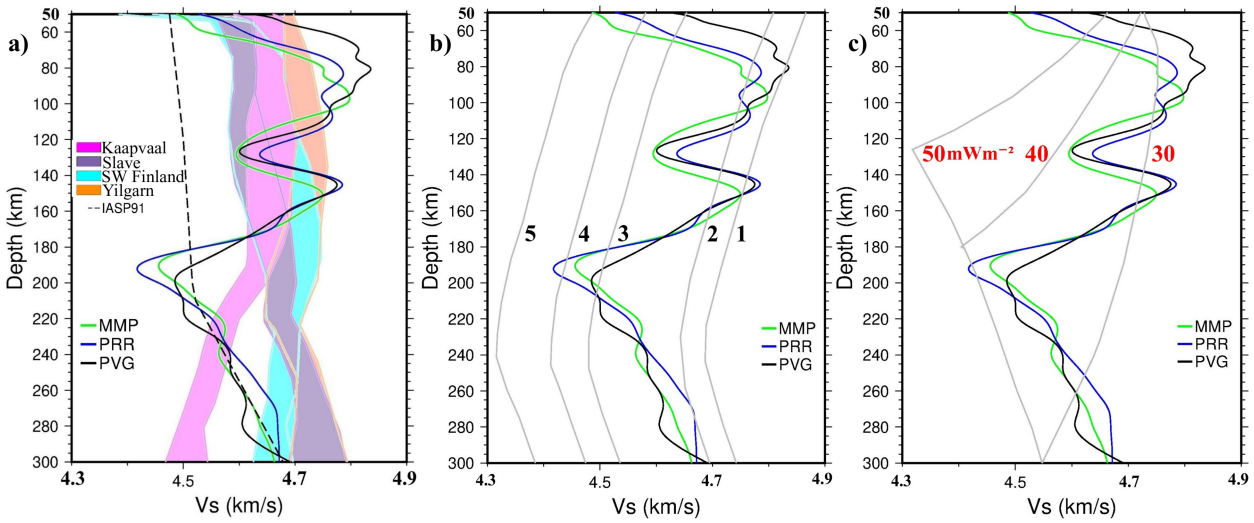

Figure 7. Shear velocity-depth models at selected stations from EDC kimberlite zone compared with (a) Velocity model for selected cratons of the world along with IASP91 (Pederson et al., 2009). (b) Theoretically computed velocity models with different mantle compositions: 1- Garnet-Spinel harzburgite (Olivine-70%), 2-Garnet lherzolite (Olivine-64.2%), 3-Garnet wehrlite (Olivine-

75.6%), 4- Amphibole peridotite (Olivine-59%) and 5-Amphibole peridotite (Olivine-50%) zone. (c) Theoretical shear wave velocity- depth model for continental thermal gradient corresponding to surface heat flow of 30, 40 and 50 mWm^{-2} assuming undepleted peridotite composition of the mantle lithosphere (Goes et al., 2020). The velocity model of the Dharwar Kimberlite zone is superimposed on the theoretical data.

6.0 Discussion

The thickness and composition of the lithosphere and the nature of the coupling between lithosphere and asthenosphere (LA) have significant implications for the longevity of cratons and understanding of important aspects of plate tectonics and geodynamics (Doglioni et al., 2011; Gerya, 2014). Cratons are underlain by thick high viscosity lithosphere. To drive plate motion, mantle convection requires coupling at the LA interface. The LA decoupling is characterized by a low viscosity layer in the asthenosphere. We discuss the properties of the LA system using shear velocity as a proxy to investigate the thermal and viscous properties of the mantle at the EDC using the velocity-depth section along the profile (Figure 8), generated through interpolating the velocity models at individual stations across the profile. The figure shows similarity in the kimberlite and non-kimberlite domain with maximum Vs $>$ 4.7 km/s in the upper lithosphere progressively decreasing to 4.6 km/s at ~170 km depth. In contrast, at the CB, a similar high velocity is observed at only shallower depths with a velocity minimum reaching 4.6 km/s at a depth of ~70 km. Detailed lithospheric- asthenosphere character is discussed below.

6.1 Lithospheric thickness and nature of LA boundary

Due to the high sensitivity of *Vs* to temperature than to composition, it has been used extensively to map Earth's mantle lithosphere. The thermal thickness of the lithosphere is considered at the depth to the intersection of the conductive geotherm and mantle adiabat (McKenzie et al., 2005; Michaut et al., 2007; Sleep, 2003), which for steady-state geotherms correspond to a minimum in seismic velocity (Goes et al., 2020). We picked the lithosphere-asthenosphere boundary (LAB) at a depth corresponding to a velocity 1.7% faster than the IASP91 velocity (Vs ~4.6 km/s) (Artemieva, 2011; Debayle & Ricard, 2012; Darbyshire et al., 2013) widely considered equivalent to the thermal boundary layer. The LAB is at a depth of ~170-180 km across EDC from west to the east (4.6 km/s contours) with a ~10-20 km thick metasomatized layer at the base. This correlates well with (a) 165 km lithospheric thickness by Mitra et al. (2006) and McKenzie et al. (2015) in the EDC, (b) 180 km using Sp conversion at nearby station HYB (Krueger et al., 2021), (c) the global lithospheric thickness of cratons 150-200 km based on heat flow and surface wave studies (Nataf & Ricard, 1996) and (d) 130-190 km using SS precursors and the deepest origin depths of diamonds (Tharimena et al., 2017). Unlike the EDC, the lithosphere is thin (80-100 km) beneath the Proterozoic Cuddapah Basin (Figure 8a), the same as inferred from the modeling of rare earth elements (Anand et al., 2003).

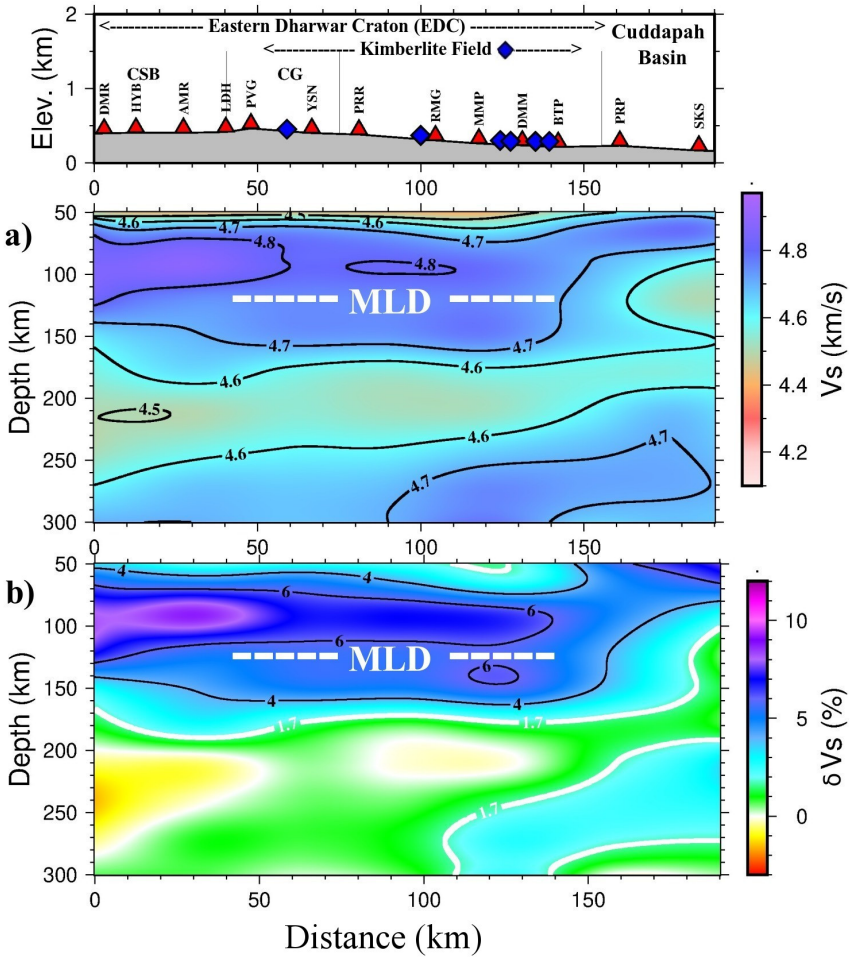

Figure 8. Velocity-depth section beneath the profile presented in Figure 1; (a) Absolute velocity, (b) Velocity perturbation relative to IASP91.

The nature of the transition from the lithosphere to the asthenosphere is much debated. The opinion is divided between a sharp and gradational velocity drop (reviewed in Doglioni et al., 2011; Mancinelli et al., 2017; Yoshida & Yoshizawa., 2021). In our study, the velocity reduces marginally from 4.6 to 4.5-4.55 km/s, a drop of 1-2% over a thickness of 60-80 km observed globally over cratons and could be explained by a very gradual vertical gradient in composition or melt (Mancinelli et al., 2017) and thereby a moderate coupling between the lithosphere and asthenosphere. The above inference of thick lithosphere and its moderate coupling with the underlying asthenosphere implies the minimum possibility of deformation of the cratonic root based on numerical experiments of Paul et al. (2019) and detailed analysis by Yoshida and Yoshizawa (2021).

6.2 Composition of the lithosphere

The velocity-depth model computed for lherzolitic to dunitic mantle composition (Bruneton et al., 2004; Eeken et al., 2018) predicts a maximum Vs of 4.8 km/s beneath the Moho at 50 km that decreases (4.65-4.75 km/s) with depth due to increase of temperature (Figure 7b). In the case of moderately metasomatized peridotite that contains phlogopite or amphibole, the Vs at 50 km depth is 4.5-4.65 km/s decreasing with depth. The velocity models at EDC kimberlite match well with the theoretically predicted velocity for the upper mantle's garnet harzburgite/webstrite composition in the depth of 70-170 km. The minimum shear velocity at a depth of 180-220 km can correspond to hydrated peridotite composition.

The kimberlite and non-kimberlite domains of EDC have similar velocities (and composition) in the lithosphere except for a more prominent 4.8 km/s layer beneath the former. We infer the highest-velocity (and by inference, lowest temperature) cores of the cratonic mantle lithosphere using a depth of positive 4% Vs anomaly (Celli et al., 2020) that corresponds to the velocity of 4.675 km/s (Figure 8b). In the western segment of EDC representing primitive craton, we observe a more than 40 km thick layer with Vs $>$ 4.8 km/s in the depth of 70-120 km, below which the velocity decreases to 4.7 and 4.6 km/s at a depth of 150 and 180 km respectively (Figure 8a). These values fall near the highest shear velocity reported for cratons globally (Hirsch et al., 2015; Garber et al., 2018; Ravenna et al., 2018). The variations in composition inferred from mantle xenoliths from kimberlites usually do not change the velocity larger than 1%. Seismological studies accounting for the radial anisotropy of minerals show that the high Vs (4.7 km/s) beneath cratons cannot be matched solely by peridotite in the depth range 100-170 km (Hirsch et al., 2015) and require an increase in the amount of garnet or eclogite in the mantle to explain such high velocity (Garber et al., 2018). Recent petrological modeling suggests that high Vs ($>$ 4.7 km/s) found in cratonic cores may require some amount of eclogite ($<$20%) and diamond (2%) in the cratonic mantle lithosphere (Garber et al., 2018). The high velocity ($Vs >$4.7 km/s) in the upper lithosphere of the Eastern Dharwar craton could be due to harzburgite-dunite composition.

At the EDC kimberlite domain, at a depth of ~130 km, we observe a negative velocity gradient where Vs reduces by 0.1 km/s from 4.7-4.75 km to 4.6 km/s, still well within the domain of an Archean craton (Figure 8). It is important to note that the region has not been subjected to any significant tectono-thermal event after 1.1 Ga even though 90 Ma kimberlite pulse, presumably related to the Marion hotspot activity, has been reported from the Wajrakarur field (Rao et al., 2016). We prefer to attribute the origin of the negative gradient or mid lithospheric discontinuity (MLD) to the process of craton formation during the Archean (Krueger et al., 2021).

6.3 Preservation of EDC lithosphere

A 160-190 km thick lithosphere is estimated from kimberlite xenoliths of the diamond-bearing field of EDC (Ganguly & Bhattacharya, 1987; Griffin et al., 2009; Shaikh et al., 2020), similar to that of present-day as indicated by our

velocity model. Also, the presence of rock assemblages like peridotite, lherzolite, harzburgite, wehrlite, dunite, and eclogites in the kimberlite xenoliths (Ganguly & Bhattacharya, 1987; Patel et al., 2009) suggests lithosphere similar to the present day harzburgite-dunite composition of the upper lithosphere of EDC indicated by Vs $>$ 4.7km/s in our velocity model. An MLD could be identified beneath the kimberlite domain, but its development is possible during craton formation in the Archean times. In the absence of any significant tectonic event, the high Vs of $>$ 4.7 km/s in the upper lithosphere in the non-kimberlite region possibly indicates a pristine Archean lithosphere. The lithosphere of the EDC both at the kimberlite and non-kimberlite regions is undisturbed by either kimberlite volcanism or any possible plume interactions except for a 10-20 km thick metasomatized layer at the base. The EDC has been moving with high velocity as part of the Indian plate since 140 Ma. Contrary to the suggestion that this might cause considerable erosion of the lithospheric root (Kumar et al., 2007, 2013; Negi et al., 1986) the EDC lithosphere has remained largely undisturbed over billions of years, supporting the continental undertow model of Alvarez (1982, 1990).

7. Conclusion

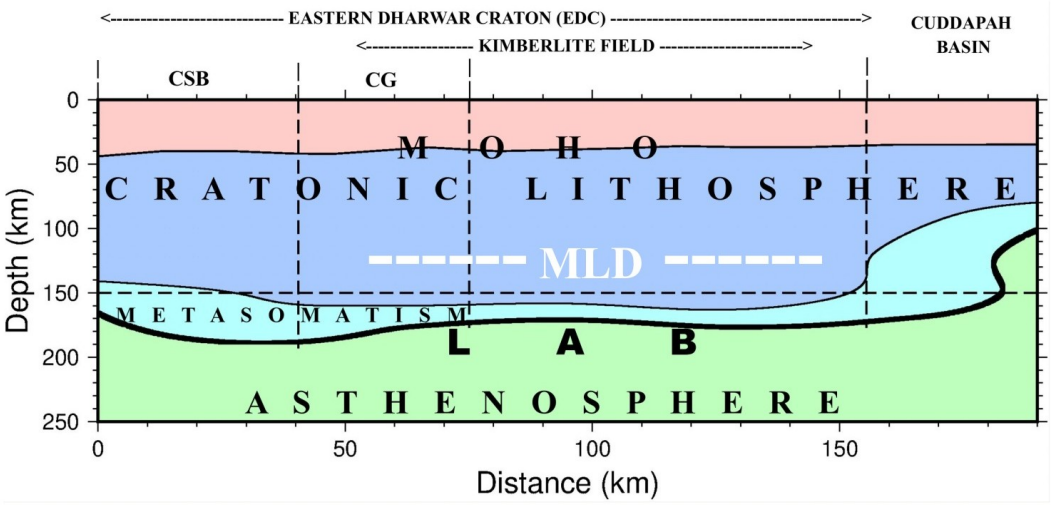

Figure 9: Interpretive geological model of the Eastern Dharwar Craton derived from the shear velocity-depth profile.

We have jointly inverted receiver function with surface wave dispersion (2-140 s) at 13 seismic stations along a 200 km long profile at the eastern part of the Dharwar craton of South India covering a non-kimberlite and a kimberlite zone. The combined surface wave-derived shear velocity structure with xenolith data from the kimberlite fields to robustly characterize the cratonic lithosphere in detail below the profile. An interpretative model has been developed (Figure 9) based on the computed velocity section (Figure 8). Our significant findings are:

1. Lithospheric thickness of ~175 km across the EDC with a ~10-20 km thick metasomatised layer at the base, and thinning to 100 km at the eastern edge of the profile below the Cuddapah basin. These results are similar to what is indicated by geochemical analysis of xenolith data representative of the lithosphere at the time of kimberlite eruption and REE modeling.

2. Very high velocity (Vsv >4.7 km/s) upper lithosphere at EDC indicates harzburgite-dunite composition, correlating well with the composition inferred from analysis of kimberlite xenolith data.

3. Evidence for thick and cold primitive cratonic lithosphere beneath the EDC that remained undisturbed at least since 1100 Ma despite kimberlite volcanism and India's interaction with mantle plumes and its fast motion.

4. The LAB at EDC is characterized by a velocity drop of ~2%, suggesting moderately low viscosity (velocity) asthenosphere below the high viscosity (velocity) craton consistent with the continental undertow model.

Acknowledgments

S.S.Rai sincerely thanks Utpal Saikia, Gokul Saha, Somasish Bose, Rishikesh Meena, and B.N.V. Prasad for their help in acquiring seismological data. D.K.Chaubey is supported by a Ph.D. fellowship from the IISER Pune. Most of the data was analyzed using Seismic Analysis Code (SAC) and all the figures were generated using Generic Mapping Tools version 5.4.5 (www.soest.hawaii.edu/gmt). The RF analysis and joint inversion were performed using Computer Programs in Seismology (https://doi.org/10.1785/0220110096).

Funding: This research is performed under the DAE- Raja Ramanna Fellowship grant (2021/ RRF/R&D II/4026). Data acquisition was made through JC Bose fellowship grant of the Department of Science & Technology, India to SSR.

Data availability

The processed receiver function data, dispersion measurement, and shear velocity model can be found at https://zenodo.org/deposit/7059808.

Credit author statement

D. K. Chaubey: Methodology, Data Curation, software, validation, analysis; **S. S. Rai:** Conceptualisation, methodology, supervision, Writing- Original draft preparation, reviewing and editing; **N. Mullick**: Resources, Writing - Review & Editing**;** and **R. Das**: Resource (ambient noise tomography).

References

Alvarez, W. (1982). Geological evidence for the geographical pattern of mantle return flow and the driving mechanism of plate tectonics. *Journal of Geophysical Research: Solid Earth*, *87*(B8), 6697-6710. https://doi.org/10.1029/JB087iB08p06697

Alvarez, W. (1990). Geologic evidence for the plate driving mechanism: The continental undertow hypothesis and the Australian Antarctic discordance. *Tectonics*, *9*(5), 1213-1220. https://doi.org/10.1029/TC009i005p01213

Ammon, C. J., Randall, G. E., & Zandt, G. (1990). On the nonuniqueness of receiver function inversions. *Journal of Geophysical Research: Solid Earth*, *95*(B10), 15303-15318. https://doi.org/10.1029/JB095iB10p15303

Ammon, C. J. (1991). The isolation of receiver effects from teleseismic P waveforms. *Bulletin-Seismological Society of America*, *81*(6), 2504-2510. https://doi.org/10.1785/BSSA0810062504

Anand, M., Gibson, S. A., Subbarao, K. V., Kelley, S. P., & Dickin, A. P. (2003). Early Proterozoic Melt Generation Processes beneath the Intra-cratonic Cuddapah Basin, Southern India. Journal of Petrology, 44(12), 2139-2171. https://doi.org/10.1093/petrology/egg073

Artemieva, I. (2011). *Lithosphere: an interdisciplinary approach*. Cambridge University Press

Bodin, T., Yuan, H., & Romanowicz, B. (2014). Inversion of receiver functions without deconvolution—application to the Indian craton. *Geophysical Journal International*, 196(2), 1025-1033. https://doi.org/10.1093/gji/ggt431

Borah, K., Rai, S. S., Priestley, K., Gaur, & V. K. (2014). The complex shallow mantle beneath the Dharwar Craton inferred from Rayleigh wave inversion. *Geophysical Journal International, 198(2), 1055-1070.* https://doi.org/10.1093/gji/ggu185

Boyd, F. R., Gurney, J. J., & Richardson, S. H. (1985). Evidence for a 150–200-km thick Archaean lithosphere from diamond inclusion thermobarometry. *Nature*, *315*(6018), 387-389. https://doi.org/10.1038/315387a0

Bruneton, M., Pedersen, H. A., Vacher, P., Kukkonen, I. T., Arndt, N. T., Funke, S., et al. (2004). Layered lithospheric mantle in the central Baltic Shield from surface waves and xenolith analysis. Earth and Planetary Science Letters, 288(1-2), 41-52, https://doi.org/10.1016/j.epsl.2004.07.034

Celli, N. L., Lebedev, S., Schaeffer, A. J., Ravenna, M., &Gaina, C. (2020). The upper mantle beneath the South Atlantic Ocean, South America and Africa from waveform tomography with massive data sets. *Geophysical Journal International*, *221*(1), 178-204. https://doi.org/10.1093/gji/ggz574

Chadwick, B., Vasudev, V.N., Hegde, G.V., 2000. The Dharwar craton, southern India, interpreted as the result of Late Archaean oblique convergence. Precambr. Res. 99 (1-2), 91–111. http://dx.doi.org/10.1016/S0301-9268(99)00055-8

Chardon, D., Jayananda, M., & Peucat, J. J. (2011). Lateral constrictional flow of hot orogenic crust: Insights from the Neoarchean of south India, geological

and geophysical implications for orogenic plateaux. *Geochemistry, Geophysics, Geosystems*, *12*(2). https://doi.org/10.1029/2010GC003398

Darbyshire, F. A., Eaton, D. W., & Bastow, I. D. (2013). Seismic imaging of the lithosphere beneath Hudson Bay: Episodic growth of the Laurentian mantle keel. *Earth and Planetary Science Letters*, *373*, 179-193. https://doi.org/10.1016/j.epsl.2013.05.002

Das, R., & Rai, S. S. (2017). Extensive seismic anisotropy in the lower crust of Archean metamorphic terrain, South India, inferred from ambient noise tomography. *Tectonophysics*, *694*, 164-180. https://doi.org/10.1016/j.tecto.2016.12.002

Debayle, E., & Ricard, Y. (2012). A global shear velocity model of the upper mantle from fundamental and higher Rayleigh mode measurements. Journal of Geophysical Research: Solid Earth, 117(B10), 10308. https://doi.org/10.1029/2012JB009288

Dipak K Chaubey. (2022). Processed receiver function data, dispersion measurement, and shear velocity model (Dharwar) [Data set]. Zenodo. https://doi.org/10.5281/zenodo.7059808

Doglioni, C., Ismail-Zadeh, A., Panza, G., & Riguzzi, F. (2011). Lithosphere–asthenosphere viscosity contrast and decoupling. *Physics of the Earth and Planetary Interiors*, *189*(1-2), 1-8. https://doi.org/10.1016/j.pepi.2011.09.006

Eeken, T., Goes, S., Pedersen, H. A., Arndt, N. T., & Bouilhol, P. (2018). Seismic evidence for depth-dependent metasomatism in cratons. *Earth and Planetary Science Letters*, *491*, 148-159. https://doi.org/10.1016/j.epsl.2018.03.018

Foley, S. F. (2008). Rejuvenation and erosion of the cratonic lithosphere. *Nature geoscience*, *1*(8), 503-510. https://doi.org/10.1038/ngeo261

Foley, S. F., Yaxley, G. M., & Kjarsgaard, B. A. (2019). Kimberlites from source to surface: insights from experiments. *Elements: An International Magazine of Mineralogy, Geochemistry, and Petrology*, *15*(6), 393-398. https://doi.org/10.2138/gselements.15.6.393

Ganguly, J., & Bhattacharya, P. K. (1987). Xenoliths in Proterozoic kimberlites from southern India: petrology and geophysical implications. *In:* P.H. Nixon (Ed.), Mantle xenoliths. John Wiley and Sons Ltd., pp.249-265.

Garber, J. M., Maurya, S., Hernandez, J. A., Duncan, M. S., Zeng, L., & Zhang, H. L. (2018). Multidisciplinary constraints on the abundance of diamond and eclogite in the cratonic lithosphere. *Geochemistry, Geophysics, Geosystems*, *19*(7), 2062-2086. https://doi.org/10.1029/2018GC007534

Gee, L. S., & Jordan, T. H. (1992). Generalized seismological data functionals. *Geophysical Journal International*, *111*(2), 363-390. https://doi.org/10.1111/j.1365-246X.1992.tb00584.x

Gerya, T. (2014). Precambrian geodynamics: concepts and models. *Gondwana Research*, *25*(2), 442-463. https://doi.org/10.1016/j.gr.2012.11.008

Goes, S., Hasterok, D., Schutt, D. L., & Klöcking, M. (2020). Continental lithospheric temperatures: A review. *Physics of the Earth and Planetary Interiors*, *306*, 106509. https://doi.org/10.1016/j.pepi.2020.106509

Goodwin, A. M. (1996). *Principles of Precambrian geology*. Elsevier.

Griffin, W. L., Kobussen, A. F., Babu, E. V. S. S. K., O'Reilly, S. Y., Norris, R., & Sengupta, P. (2009). A translithospheric suture in the vanished 1-Ga lithospheric root of South India: evidence from contrasting lithosphere sections in the Dharwar Craton. *Lithos*, *112*, 1109-1119. https://doi.org/10.1016/j.lithos.2009.05.015

Gurrola, H., Baker, G. E., & Minster, J. B. (1995). Simultaneous time-domain deconvolution with application to the computation of receiver functions. *Geophysical Journal International*, *120*(3), 537-543. https://doi.org/10.1111/j.1365-246X.1995.tb01837.x

Hawkesworth, C. J., Kempton, P. D., Rogers, N. W., Ellam., R.M., & van Calsteren, P. W. (1990). Continental mantle lithosphere, and shallow level enrichment processes in the Earth's mantle. Earth and Planetary Science Letters, 96(3-4), 256-268. https://doi.org/10.1016/0012-821X(90)90006-J

Herrmann, R. B. (2013). Computer programs in seismology: An evolving tool for instruction and research. *Seismological Research Letters*, *84*(6), 1081-1088. https://doi.org/10.1785/0220110096

Hirsch, A. C., Dalton, C. A., & Ritsema, J. (2015). Constraints on shear velocity in the cratonic upper mantle from Rayleigh wave phase velocity. *Geochemistry, Geophysics, Geosystems*, *16*(11), 3982-4005. https://doi.org/10.1002/2015GC006066

Jayananda, M., Aadhiseshan, K. R., Kusiak, M. A., Wilde, S. A., Sekhamo, K. U., Guitreau, M., ... & Gireesh, R. V. (2020). Multi-stage crustal growth and Neoarchean geodynamics in the Eastern Dharwar Craton, southern India. *Gondwana Research*, *78*, 228-260. https://doi.org/10.1016/j.gr.2019.09.005

Jin, G., & Gaherty, J. B. (2015). Surface wave phase-velocity tomography based on multichannel cross-correlation. *Geophysical Journal International*, *201*(3), 1383-1398. https://doi.org/10.1093/gji/ggv079

Jordan, T. H. (1979). Mineralogies, densities and seismic velocities of garnet lherzolites and their geophysical implications. *The mantle sample: Inclusion in kimberlites and other volcanics*, *16*, 1-14. https://doi.org/10.1029/SP016p0001

Jordan, T. H. (1988). Structure and formation of the continental tectosphere. *Journal of Petrology*, (1), 11-37. https://doi.org/10.1093/petrology/Special_Volume.1.11

Julia, J., Ammon, C. J., Herrmann, R. B., & Correig, A. M. (2000). Joint inversion of receiver function and surface wave dispersion observations. *Geophysical Journal International*, *143*(1), 99-112. https://doi.org/10.1046/j.1365-246x.2000.00217.x

Kosarev, G. L., Oreshin, S. I., Vinnik, L. P., Kiselev, S. G., Dattatrayam, R. S., Suresh, G., & Baidya, P. R. (2013). Heterogeneous lithosphere and the underlying mantle of the Indian subcontinent. Tectonophysics, 592, 175-186. https://doi.org/10.1016/j.tecto.2013.02.023

Krueger, H. E., Gama, I., & Fischer, K. M. (2021). Global Patterns in Cratonic Mid-Lithospheric Discontinuities FromSp Receiver Functions. *Geochemistry, Geophysics, Geosystems*, *22*(6), e2021GC009819. https://doi.org/10.1029/2021GC009819

Kumar, A., Heaman, L. M., & Manikyamba, C. (2007). Mesoproterozoic kimberlites in south India: A possible link to 1.1 Ga global magmatism. *Precambrian Research*, *154*(3-4), 192-204. https://doi.org/10.1016/j.precamres.2006.12.007

Kumar, P., Yuan, X., Kumar, M. R., Kind, R., Li, X., & Chadha, R. K. (2007). The rapid drift of the Indian tectonic plate. *Nature*, *449*(7164), 894-897. https://doi.org/10.1038/nature06214

Kumar, P., Ravi Kumar, M., Srijayanthi, G., Arora, K., Srinagesh, D., Chadha, R. K., & Sen, M. K. (2013). Imaging the lithosphere-asthenosphere boundary of the Indian plate using converted wave techniques. *Journal of Geophysical Research: Solid Earth*, *118*(10), 5307-5319. https://doi.org/10.1002/jgrb.50366

Langston, C. A. (1977). The effect of planar dipping structure on source and receiver responses for constant ray parameter. *Bulletin of the Seismological Society of America*, *67*(4), 1029-1050. https://doi.org/10.1785/BSSA0670030713

Lee, C. A., Luffi, P., & Chin E. J. (2011). Building and Destroying Continental Mantle. Annual Review of Earth and Planetary Sciences, 39, 59-90. https://doi.org/10.1146/annurev-earth-040610-133505

Lenardic, A., Moresi, L., & Mühlhaus, H. (2000). The role of mobile belts for the longevity of deep cratonic lithosphere: the crumple zone model. *Geophysical Research Letters*, *27*(8), 1235-1238. https://doi.org/10.1029/1999GL008410

Lenardic, A., Moresi, L. N., & Mühlhaus, H. (2003). Longevity and stability of cratonic lithosphere: insights from numerical simulations of coupled mantle convection and continental tectonics. *Journal of Geophysical Research: Solid Earth*, *108*(B6). https://doi.org/10.1029/2002JB001859

Ligorría, J. P., & Ammon, C. J. (1999). Iterative deconvolution and receiver-function estimation. *Bulletin of the seismological Society of America*, *89*(5), 1395-1400. https://doi.org/10.1785/BSSA0890051395

Liu, M., & Li, Z. (2018). Dynamics of thinning and destruction of the continental cratonic lithosphere: Numerical modeling. Science China Earth Sciences, 61(7), 823-852. https://doi.org/10.1007/s11430-017-9184-x

Mancinelli, N. J., Fischer, K. M., & Dalton, C. A. (2017). How sharp is the cratonic lithosphere-asthenosphere transition?.*Geophysical Research Letters*, *44*(20), 10-189. https://doi.org/10.1002/2017GL074518

Maurya, S., Montagner, J. P., Kumar, M. R., Stutzmann, E., Kiselev, S., Burgos, G., et al. (2016). Imaging the lithospheric structure beneath the Indian continent. *Journal of Geophysical Research: Solid Earth*, *121*(10), 7450-7468. https://doi.org/10.1002/2016JB012948

McKenzie, D., Jackson, J., & Priestley, K. (2005). Thermal structure of oceanic and continental lithosphere. *Earth and Planetary Science Letters*, *233*(3-4), 337-349. https://doi.org/10.1016/j.epsl.2005.02.005

McKenzie, D., Daly, M. C., & Priestley, K. (2015). The lithospheric structure of Pangea. *Geology*, *43*(9), 783-786. https://doi.org/10.1130/G36819.1

Meier, U., Curtis, A., & Trampert, J. (2007). A global crustal model constrained by nonlinearised inversion of fundamental mode surface waves. *Geophysical Research Letters*, *34*, L16304. https://doi.org/10.1029/2007gl030989

Michaut, C., Jaupart, C., & Bell, D. R. (2007). Transient geotherms in Archean continental lithosphere: New constraints on thickness and heat production of the subcontinental lithospheric mantle. *Journal of Geophysical Research: Solid Earth*, *112*(B4). https://doi.org/10.1029/2006JB004464

Mitra, S., Priestley, K., Gaur, V. K., Rai, S. S., & Haines, J. (2006). Variation of Rayleigh wave group velocity dispersion and seismic heterogeneity of the Indian crust and uppermost mantle. *Geophysical Journal International*, *164*(1), 88-98. https://doi.org/10.1111/j.1365-246X.2005.02837.x

Mullick, N., Rai, S. S., & Saha, G. (2022). Lithospheric structure of the South India Precambrian terrains from surface wave tomography. *Journal of Geophysical Research: Solid Earth*, e2022JB024244. https://doi.org/10.1029/2022JB024244

Naqvi, S. M., & Rogers, J. J. W. (1987). *Precambrian geology of India*. Oxford University Press, USA.

Nataf, H.-C., & Ricard Y. (1996). 3SMAC: an a priori tomographic model of the upper mantle based on geophysical modeling. Physics of the Earth and Planetary Interiors, 95, 101-122. https://doi.org/10.1016/0031-9201(95)03105-7

Negi, J. G., Pandey, O. P., & Agrawal, P. K. (1986). Super-mobility of hot Indian lithosphere. *Tectonophysics*, *131*(1-2), 147-156. https://doi.org/10.1016/0040-1951(86)90272-6

Oreshin, S. I., Vinnik, L. P., Kiselev, S. G., Rai, S. S., Prakasam, K. S., & Treussov, A. V. (2011). Deep seismic structure of the Indian shield, western

Himalaya, Ladakh and Tibet. *Earth and Planetary Science Letters,* 307(3-4), 415-429. https://doi.org/10.1016/j.epsl.2011.05.016

Park, J., & Levin, V. (2000). Receiver functions from multiple-taper spectral correlation estimates. *Bulletin of the Seismological Society of America*, *90*(6), 1507-1520. https://doi.org/10.1785/0119990122

Patel, S. C., Ravi, S., Anil kumar, Y., Naik, A., Thakur, S. S., Pati, J. K., & Nayak, S. S. (2009). Mafic xenoliths in Proterozoic kimberlites from Eastern Dharwar Craton, India: mineralogy and P–T regime. *Journal of Asian Earth Sciences*, *34*(3), 336-346. https://doi.org/10.1016/j.jseaes.2008.06.001

Paul, J., Ghosh, A., & Conrad, C. P. (2019). Traction and strain-rate at the base of the lithosphere: an insight into cratonic survival. *Geophysical Journal International*, *217*(2), 1024-1033. https://doi.org/10.1093/gji/ggz079

Pearson, D. G., Woodhead, J., & Janney, P. E. (2019). Kimberlites as geochemical probes of Earth's mantle. *Elements: An International Magazine of Mineralogy, Geochemistry, and Petrology*, *15*(6), 387-392. https://doi.org/10.2138/gselements.15.6.387

Pearson, D. G., Scott, J. M., Liu, J., Schaeffer, A., Wang, L. H., van Hunen, J., et al. (2021). Deep continental roots and cratons. Nature, 596, 199-210. https://doi.org/10.1038/s41586-021-03600-5

Pedersen, H. A., Fishwick, S., & Snyder, D. B. (2009). A comparison of cratonic roots through consistent analysis of seismic surface waves. *Lithos*, *109*(1-2), 81-95. https://doi.org/10.1016/j.lithos.2008.09.016

Peucat, J. J., Jayananda, M., Chardon, D., Capdevila, R., Fanning, C. M., & Paquette, J. L. (2013). The lower crust of the Dharwar Craton, Southern India: Patchwork of Archean granulitic domains. *Precambrian Research*, *227*, 4-28. https://doi.org/10.1016/j.precamres.2012.06.009

Priestley, K., & McKenzie, D. (2006). The thermal structure of the lithosphere from shear wave velocities. *Earth and Planetary Science Letters*, *244*(1-2), 285-301. https://doi.org/10.1016/j.epsl.2006.01.008

Priestley, K., Ho, T., & McKenzie, D. (2021). The formation of continental roots. *Geology*, *49*(2), 190-194. https://doi.org/10.1130/G47696.1

Rai, S. S., Borah, K., Das, R., Gupta, S., Srivastava, S., Prakasam, K. S., et al. (2013). The south India Precambrian crust and shallow lithospheric mantle: Initial results from the India Deep Earth Imaging Experiment (INDEX). *Journal of Earth System Science*, *122*(6), 1435-1453. https://doi.org/10.1007/s12040-013-0357-0

Ramakrishnan, M., & Nath, J. S. (Eds.). (1981). *Early Precambrian supracrustals of southern Karnataka* (Vol. 112). Geological Survey of India.

Rao N.V.C., Dongre, A.N., Wu, F.Y and Lehmann, B. (2016) A Late Cretaceous (ca. 90 Ma) kimberlite event in southern India: Implication for sub-continental

lithospheric mantle evolution and diamond exploration. Gondwana Research v. 35, pp. 378-389. https://doi.org/10.1016/j.gr.2015.06.006

Ravenna, M., Lebedev, S., Fullea, J., & Adam, J. M. C. (2018). Shear wave velocity structure of Southern Africa's lithosphere: Variations in the thickness and composition of cratons and their effect on topography. *Geochemistry, Geophysics, Geosystems*, *19*(5), 1499-1518. https://doi.org/10.1029/2017GC007399

Ritzwoller, M. (2014), Ambient noise seismic imaging, inMcGraw Hill Year Book on Science and Technology, pp. 1–13, McGraw-Hill, New York.

Roy, S., & Rao, R. U. M. (2000). Heat flow in the Indian shield. Journal of Geophysical Research: Solid Earth, 105(B11), 25587-25604. https://doi.org/10.1029/2000JB900257

Saha, G. K., Prakasam, K. S., & Rai, S. S. (2020). Diversity in the peninsular Indian lithosphere revealed from ambient noise and earthquake tomography. *Physics of the Earth and Planetary Interiors,* 306, 106523. https://doi.org/10.1016/j.pepi.2020.106523

Saikia, U., Das, R., & Rai, S. S. (2017). Possible magmatic underplating beneath the west coast of India and adjoining Dharwar craton: Imprint from Archean crustal evolution to breakup of India and Madagascar. *Earth and Planetary Science Letters*, *462*, 1-14. https://doi.org/10.1016/j.epsl.2017.01.004

Saikia, U., & Rai, S. S. (2018). Seismicity Pattern, Reference Velocity Model, and Earthquake Mechanics of South India. *Bulletin of the Seismological Society of America*, *108*(1), 116-129. https://doi.org/10.1785/0120160369

Salaün, G., Pedersen, H. A., Paul, A., Farra, V., Karabulut, H., Hatzfeld, D., ... & SIMBAAD team. (2012). High-resolution surface wave tomography beneath the Aegean-Anatolia region: constraints on upper-mantle structure. *Geophysical Journal International*, *190*(1), 406-420. https://doi.org/10.1111/j.1365-246X.2012.05483.x

Schutt, D. L., & Lesher, C. E. (2006). Effects of melt depletion on the density and seismic velocity of garnet and spinel lherzolite. *Journal of Geophysical Research: Solid Earth*, *111*(B5). https://doi.org/10.1029/2003JB002950

Shaikh, A. M., Tappe, S., Bussweiler, Y., Patel, S. C., Ravi, S., Bolhar, R., & Viljoen, F. (2020). Clinopyroxene and garnet mantle cargo in kimberlites as probes of Dharwar craton architecture and geotherms, with implications for post-1.1 Ga lithosphere thinning events beneath southern India. *Journal of Petrology*, *61*(9), egaa087. https://doi.org/10.1093/petrology/egaa087

Shapiro, N. M., & Ritzwoller, M. H. (2002). Monte-Carlo inversion for a global shear-velocity model of the crust and upper mantle. *Geophysical Journal International*, *151*(1), 88-105. https://doi.org/10.1046/j.1365-246X.2002.01742.x

Sleep, N. H. (2003). Survival of Archean cratonal lithosphere. *Journal of Geophysical Research: Solid Earth*, *108*(B6). https://doi.org/10.1029/2001JB0001

69

Sleep, N. H. (2005). Evolution of the continental lithosphere. *Annual Review of Earth and Planetary Sciences,* 33(1), 369-393. https://doi.org/10.1146/annurev.earth.33.092203.122643

Tharimena, S., Rychert, C., & Harmon, N. (2017). A unified continental thickness from seismology and diamonds suggests a melt-defined plate. *Science*, *357*(6351), 580-583. https://doi.org/10.1126/science.aan0741

Wu, F., Xu, Y., Zhu, R., & Zhang, G. (2014). Thinning and destruction of the cratonic lithosphere: A global perspective. *Science China Earth Sciences*, *57*(12), 2878-2890. https://doi.org/10.1007/s11430-014-4995-0

Yoshida, M., &Yoshizawa, K. (2021). Continental drift with deep cratonic roots. *Annual Review of Earth and Planetary Sciences*, *49*, 117-139. https://doi.org/10.1146/annurev-earth-091620-113028